Energy Proceedings
Vol 26, 2022
ISSN 2004-2965

Island Partition-Based Recovery of AC/DC Hybrid Distribution Network with Coordination of Multiple Sources#

Chaoxian Lv[1*], Chengxu Zhu[1], Xiaotong Zhang[1], Wei Jin[1]

1 School of Electrical Engineering, China University of Mining and Technology, Xuzhou 221116, China

(Corresponding Author: chaoxianlv@163.com)

ABSTRACT

This paper proposes a fault recovery strategy for AC/DC hybrid distribution networks (HDNs) to restore critical loads in face of extreme events, in which the flexible topology with islanding partition is integrated for multi-source synergy. The island partition-based recovery model maximizes the active power of restored loads as the objective function while considering the power flow constraints, radial topology constraints, and multiple sources' constraints. Then, the proposed model is transformed into a mixed-integer second-order cone programming (MISOCP) formulation by linearization and convex relaxation, which can be solved effectively. Finally, the effectiveness of the proposed service restoration method is validated on a modified IEEE 33-node AC/DC test feeder.

Keywords: fault recovery, island partition, AC/DC hybrid distribution network (HDN), mixed-integer second-order cone programming (MISOCP)

NONMENCLATURE

Abbreviations	
CDG	Controllable distributed generator
ESS	Energy storage system
VSC	Voltage source converter
HDN	AC/DC hybrid distribution network
MISOCP	Mixed-integer second-order cone programming
Symbols	
Ω_{n}	Set of all nodes
Ω_{b}	Set of all branches
$\Omega_{\mathrm{AC}}/\Omega_{\mathrm{DC}}$	Set of AC/DC branches
Ω_{s}	Set of nodes that can provide voltage support for formed islands
Ω_{t}	Set of periods of islanding time horizon

1. INTRODUCTION

Extreme events in power grids can result in severe power disruptions and economic losses among customers and utilities [1]. It is reported that power faults in distribution networks account for more than 90% of the total power outages [2]. As a result, post-fault supply restoration is essential in improving the reliability of distribution networks, and it is indispensable to present a supply restoration schedule that can restore loads efficiently and quickly [3].

Lots of papers have studied the fault recovery problems of alternating current (AC) distribution networks. In [4], a multi-stage restoration method is employed to maximize the amount of load restored by distributed generators (DGs). The restoration scheme proposed in [5] establishes a multi-objective optimization model and studies the influence of the vehicle-to-grid facility on supply restoration.

With the development of power electronic components and flexible direct current (DC) transmission technology, the DC distribution technology based on the voltage source converter (VSC) has been widely employed in distribution networks. In the case of high integration of renewable energy, the AC/DC hybrid distribution network (HDN) has significant advantages over the AC distribution network in terms of reliability. The traditional AC distribution network is gradually transformed into the HDN in places [6], [7].

The network structure and operation mode of the HDN is more complex than the traditional AC system, Therefore, common service restoration methods designed for AC distribution networks are not applicable to the special grid structure and electrical characteristics in HDNs. In [8], a fault recovery optimization model is proposed, which concentrates on analyzing the differences between HDNs and traditional AC distribution networks in two aspects of objective functions and constraint conditions. But the proposed method does not consider the coordination of multiple

resources such as controllable distributed generators (CDGs) or energy storage systems (ESSs) in different fault fields, and the support of alternative reconfiguration for the fault recovery of AC/DC networks has also not been involved.

The work presented in this paper establishes an optimal network reconfiguration model of HDNs, facilitating the coordination of multiple controllable resources to restore critical loads. Compared with the state-of-the-art, the major contributions of the paper include:

1) Based on the islanding partition strategy, several isolated and self-sustainable islands energized by local DGs or ESSs are formed. Through the exchange of active power between AC networks and DC networks to balance the total load better.

2) The mixed-integer second-order cone programming (MISOCP) is applied to solve the optimization model with fast and stable computational performance.

2. FAULT RECOVERY MODEL OF AC/DC HYBRID DISTRIBUTION

2.1 Objective function

This paper takes the maximization of active power of restored loads as the objective function, which is formulated as follows:

$$f = \max \sum_{t\in\Omega_{\mathrm{t}}} \sum_{i\in\Omega_{\mathrm{n}}} \lambda_i \omega_i P_{t,i}^{\mathrm{L}} \tag{1}$$

where λ_i is a binary variable associated with restored coefficient at node i; $\lambda_i = 1$ implies that load at node i is totally restored, while $\lambda_i = 0$ implies that load at node i is not recovered; ω_i is the weight coefficient of load importance at node i; $P_{i,t}^{\mathrm{L}}$ is the active power consumption at node i and time t.

2.2 Power flow constraints

2.2.1 AC power flow constraints

$$\sum_{ij\in\Omega_{\mathrm{AC}}} \left(P_{\mathrm{AC},ij,t} - R_{ij} I_{\mathrm{AC},ij,t}^2\right) + P_{\mathrm{AC},j,t} = \sum_{jk\in\Omega_{\mathrm{AC}}} P_{\mathrm{AC},jk,t} \tag{2}$$

$$\sum_{ij\in\Omega_{\mathrm{AC}}} \left(Q_{\mathrm{AC},ij,t} - X_{ij} I_{\mathrm{AC},ij,t}^2\right) + Q_{\mathrm{AC},j,t} = \sum_{jk\in\Omega_{\mathrm{AC}}} Q_{\mathrm{AC},jk,t} \tag{3}$$

$$P_{\mathrm{AC},j,t} = P_{j,t}^{\mathrm{CDG}} - \lambda_i P_{\mathrm{AC},j,t}^{\mathrm{L}} \tag{4}$$

$$Q_{\mathrm{AC},j,t} = Q_{j,t}^{\mathrm{CDG}} - \lambda_i Q_{\mathrm{AC},j,t}^{\mathrm{L}} \tag{5}$$

$$U_{\mathrm{AC},i,t}^2 - U_{\mathrm{AC},j,t}^2 - 2\left(R_{ij} P_{\mathrm{AC},ij,t} + X_{ij} Q_{\mathrm{AC},ij,t}\right) + \left(R_{ij}^2 + X_{ij}^2\right) I_{\mathrm{AC},ij,t}^2 + \mathrm{M}\left(1 - \alpha_{\mathrm{AC},ij}\right) \geq 0 \tag{6}$$

$$U_{\mathrm{AC},i,t}^2 - U_{\mathrm{AC},j,t}^2 - 2\left(R_{ij} P_{\mathrm{AC},ij,t} + X_{ij} Q_{\mathrm{AC},ij,t}\right) + \left(R_{ij}^2 + X_{ij}^2\right) I_{\mathrm{AC},ij,t}^2 - \mathrm{M}\left(1 - \alpha_{\mathrm{AC},ij}\right) \leq 0 \tag{7}$$

$$U_{\mathrm{AC},i,t}^2 I_{\mathrm{AC},ij,t}^2 = P_{\mathrm{AC},ij,t}^2 + Q_{\mathrm{AC},ij,t}^2 \tag{8}$$

$$0 \leq I_{\mathrm{AC},ij,t}^2 \leq \mathrm{M}\alpha_{\mathrm{AC},ij} \tag{9}$$

$$-\mathrm{M}\alpha_{\mathrm{AC},ij} \leq P_{\mathrm{AC},ij,t} \leq \mathrm{M}\alpha_{\mathrm{AC},ij} \tag{10}$$

$$-\mathrm{M}\alpha_{\mathrm{AC},ij} \leq Q_{\mathrm{AC},ij,t} \leq \mathrm{M}\alpha_{\mathrm{AC},ij} \tag{11}$$

where $P_{\mathrm{AC},ij,t}/Q_{\mathrm{AC},ij,t}$ is the active/reactive power flow of AC branch ij at time t; $P_{\mathrm{AC},j,t}/Q_{\mathrm{AC},j,t}$ is the total active /reactive power injection at AC node j and time t; $P_{j,t}^{\mathrm{CDG}}/Q_{j,t}^{\mathrm{CDG}}$ is the active/reactive power injection by CDG at AC node j and time t; $P_{\mathrm{AC},j,t}^{\mathrm{L}}/Q_{\mathrm{AC},j,t}^{\mathrm{L}}$ is the active/reactive power consumption at AC node j and time t; $U_{\mathrm{AC},i,t}^2$ is the squared voltage magnitude at AC node i and time t; $I_{\mathrm{AC},ij,t}^2$ is the squared current magnitude of AC branch ij at time t.

2.2.2 DC power flow constraints

$$\sum_{mn\in\Omega_{\mathrm{DC}}} \left(P_{\mathrm{DC},mn,t} - R_{mn} I_{\mathrm{DC},mn,t}^2\right) + P_{\mathrm{DC},n,t} = \sum_{nk\in\Omega_{\mathrm{DC}}} P_{\mathrm{DC},nk,t} \tag{12}$$

$$P_{\mathrm{DC},n,t} = P_{n,t}^{\mathrm{PV}} + P_{n,t}^{\mathrm{dis}} - P_{n,t}^{\mathrm{ch}} - \lambda_i P_{\mathrm{DC},n,t}^{\mathrm{L}} \tag{13}$$

$$U_{\mathrm{DC},m,t}^2 - U_{\mathrm{DC},n,t}^2 - 2R_{mn} P_{\mathrm{DC},mn,t} + R_{mn}^2 I_{\mathrm{DC},mn,t}^2 + \mathrm{M}\left(1 - \alpha_{\mathrm{DC},mn}\right) \geq 0 \tag{14}$$

$$U_{\mathrm{DC},m,t}^2 - U_{\mathrm{DC},n,t}^2 - 2R_{mn} P_{\mathrm{DC},mn,t} + R_{mn}^2 I_{\mathrm{DC},mn,t}^2 - \mathrm{M}\left(1 - \alpha_{\mathrm{DC},mn}\right) \leq 0 \tag{15}$$

$$U_{\mathrm{DC},m,t}^2 I_{\mathrm{DC},mn,t}^2 = P_{\mathrm{DC},mn,t}^2 \tag{16}$$

$$0 \leq I_{\mathrm{DC},mn,t}^2 \leq \mathrm{M}\alpha_{\mathrm{DC},mn} \tag{17}$$

$$-\mathrm{M}\alpha_{\mathrm{DC},mn} \leq P_{\mathrm{DC},mn,t} \leq \mathrm{M}\alpha_{\mathrm{DC},mn} \tag{18}$$

where $P_{\mathrm{DC},mn,t}$ is the active power flow of DC branch mn at time t; $P_{\mathrm{DC},n,t}$ is the total active power injection at DC node n and time t; $P_{n,t}^{\mathrm{PV}}$ is the active power injection by PV at DC node n and time t; $P_{n,t}^{\mathrm{ch}}/P_{n,t}^{\mathrm{dis}}$ is the charging/discharging power by ESS at DC node n and time t; $P_{\mathrm{DC},n,t}^{\mathrm{L}}$is the active power consumption at DC node n and time t; $U_{\mathrm{DC},m,t}^2$ is the squared voltage magnitude at DC node m and time t; $I_{\mathrm{DC},mn,t}^2$ is the squared current magnitude of DC branch mn at time t.

2.2.3 Operation constraints of VSCs

For the HDN, DC distribution networks are linked to AC distribution networks through VSC stations, achieving the power conversion between both sides. As shown in Fig. 1, a simplified equivalent circuit model of the VSC station is established. Meanwhile, this paper models the

electrical equipment between the AC side of the VSC station and the point of common coupling as series impedance [9].

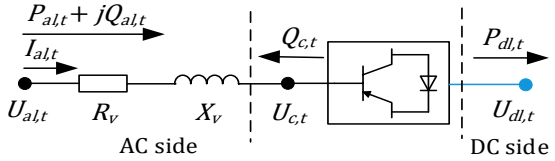

Fig. 1 Equivalent circuit of VSC

In this figure, $P_{al,t}/Q_{al,t}$ is the active/reactive power flow on the AC side of the VSC station at time t; $P_{dl,t}$ is the active power flow on the DC side of the VSC station at time t; $Q_{c,t}$ is the reactive power injection by VSC at time t; $U_{al,t}, U_{c,t}, U_{dl,t}$ are the voltage magnitude on the AC side, equivalent internal potential and voltage magnitude on the DC side, respectively [10]. The associated active and reactive power flow can be calculated as follows:

$$P_{al,t} - I_{al,t}^2 R_v = P_{dl,t} \tag{19}$$

$$Q_{al,t} - I_{al,t}^2 X_v = -Q_{c,t} \tag{20}$$

$$Q_{\mathrm{VSC,min}} \le Q_{c,t} \le Q_{\mathrm{VSC,max}} \tag{21}$$

where $Q_{\mathrm{VSC,max}}/Q_{\mathrm{VSC,min}}$ is the upper/lower limit of reactive power provided by VSC; $I_{al,t}$ is the current magnitude on the AC side of the VSC station at time t.

The relation of voltage magnitude between the AC side and the DC side of the VSC station is presented as follows:

$$U_{c,t} = \mathrm{K_{vsc}} M_v U_{d,t} \tag{22}$$

$$0.9U_{d,t} \le U_{c,t} \le U_{d,t} \tag{23}$$

where $\mathrm{K_{vsc}}$ depends on the type of VSC and the control strategy of PWM, which is set as $\sqrt{3}/2\sqrt{2}$; M_v is the modulation index; when the relation of $U_{\mathrm{base}}^{\mathrm{ac}}$ and $U_{\mathrm{base}}^{\mathrm{dc}}$ is $U_{\mathrm{base}}^{\mathrm{ac}} = \mathrm{K_{vsc}} U_{\mathrm{base}}^{\mathrm{dc}}$, $M_v \in \left[U_{\mathrm{ac.p.u}}^{\min}/U_{\mathrm{dc.p.u}}^{\max}, 1\right]$, constraint (22) is convert to constraint (23) [11].

2.3 Topology constraints

$$\beta_{ij} + \beta_{ji} = \alpha_{ij},\ ij \in \Omega_{\mathrm{b}} \tag{24}$$

$$\sum_{ij\in\Omega_{\mathrm{b}}} \beta_{ij} = 1,\ \forall i \in \Omega_{\mathrm{n}} \backslash \Omega_{\mathrm{s}} \tag{25}$$

$$\sum_{ij\in\Omega_{\mathrm{b}}} \beta_{ij} = 0,\ \forall i \in \Omega_{\mathrm{s}} \tag{26}$$

$$\alpha_{ij}, \beta_{ij}, \beta_{ji} \in \{0,1\} \tag{27}$$

where α_{ij} is a binary variable and denotes the state of switch in branch ij; the value of α_{ij} is 1 if the switch is closed; otherwise α_{ij} is 0. β_{ij} is a binary variable; the value of β_{ij} is 1 if node j is the parent of node i; otherwise β_{ij} is 0.

For the nodes in the fault area, constraint (25) indicates each node has only one parent node to ensure that there will be only one node to provide voltage support in the fault area. Constraint (26) represents that node i is chosen to provide voltage support in the formed island.

2.4 System operation constraints

$$\left(U_{\mathrm{AC}}^{\min}\right)^2 \le U_{\mathrm{AC},i,t}^2 \le \left(U_{\mathrm{AC}}^{\max}\right)^2 \tag{28}$$

$$\left(U_{\mathrm{DC}}^{\min}\right)^2 \le U_{\mathrm{DC},m,t}^2 \le \left(U_{\mathrm{DC}}^{\max}\right)^2 \tag{29}$$

$$0 \le I_{\mathrm{AC},ij,t}^2 \le \left(I_{\mathrm{AC}}^{\max}\right)^2 \tag{30}$$

$$0 \le I_{\mathrm{DC},mn,t}^2 \le \left(I_{\mathrm{DC}}^{\max}\right)^2 \tag{31}$$

where $U_{\mathrm{AC}}^{\max}/U_{\mathrm{AC}}^{\min}$ is the upper/lower limit of AC system voltage; $U_{\mathrm{DC}}^{\max}/U_{\mathrm{DC}}^{\min}$ is the upper/lower limit of DC system voltage; $I_{\mathrm{AC}}^{\max}/I_{\mathrm{DC}}^{\max}$ is the upper limit of AC/DC system current.

2.5 Operation constraints of CDGs

$$P_i^{\mathrm{CDG,min}} \le P_{i,t}^{\mathrm{CDG}} \le P_i^{\mathrm{CDG,max}} \tag{32}$$

$$-\frac{P_{i,t}^{\mathrm{CDG}}\sqrt{1-\left(\kappa_i^{\min}\right)^2}}{\kappa_i^{\min}} \le Q_{i,t}^{\mathrm{CDG}} \le \frac{P_{i,t}^{\mathrm{CDG}}\sqrt{1-\left(\kappa_i^{\min}\right)^2}}{\kappa_i^{\min}} \tag{33}$$

$$\sqrt{\left(P_{i,t}^{\mathrm{CDG}}\right)^2 + \left(Q_{i,t}^{\mathrm{CDG}}\right)^2} \le S_i^{\mathrm{CDG}} \tag{34}$$

where $P_i^{\mathrm{CDG,max}}, P_i^{\mathrm{CDG,min}}$ is the upper/lower limit of active power provided by CDG; κ is the power factor of CDG; S_i^{CDG} is the capacity of CDG.

2.6 Operation constraints of PVs

$$0 \le P_{n,t}^{\mathrm{PV}} \le P_t^{\mathrm{PV},0} \tag{35}$$

where $P_t^{\mathrm{PV},0}$ is the upper limit of active power provided by PV.

2.7 Operation constraints of ESSs

$$y_{n,t}^{\mathrm{ch}} + y_{n,t}^{\mathrm{dis}} \le 1 \tag{36}$$

$$y_{n,t}^{\mathrm{ch}} P_{n,t}^{\mathrm{ch,min}} \le P_{n,t}^{\mathrm{ch}} \le y_{n,t}^{\mathrm{ch}} P_{n,t}^{\mathrm{ch,max}} \tag{37}$$

$$y_{n,t}^{\mathrm{dis}} P_{n,t}^{\mathrm{dis,min}} \le P_{n,t}^{\mathrm{dis}} \le y_{n,t}^{\mathrm{dis}} P_{n,t}^{\mathrm{dis,max}} \tag{38}$$

$$E_{n,t+1}^{\mathrm{ESS}} = E_{n,t}^{\mathrm{ESS}} + \eta^{\mathrm{ch}} P_{n,t}^{\mathrm{ch}} - P_{n,t}^{\mathrm{dis}}/\eta^{\mathrm{dis}} \tag{39}$$

$$E_n^{\mathrm{ESS,min}} \le E_{n,t}^{\mathrm{ESS}} \le E_n^{\mathrm{ESS,max}} \tag{40}$$

where $y_{n,t}^{\mathrm{ch}}/y_{n,t}^{\mathrm{dis}}$ is a binary variable associated with the charging/discharging status of ESS; $P_{n,t}^{\mathrm{ch,max}}/P_{n,t}^{\mathrm{ch,min}}$ is the upper/lower limit of charging power; $P_{n,t}^{\mathrm{dis,max}}/$

$P_{n,t}^{\mathrm{dis,min}}$ is the upper/lower limit of discharging power; $E_n^{\mathrm{ESS,max}}/E_n^{\mathrm{ESS,min}}$ is the upper/lower limit of energy storage of ESS; $\eta^{\mathrm{ch}}/\eta^{\mathrm{dis}}$ is the charging/discharging efficiency.

2.8 Second-order cone conversion

For power flow constraints, auxiliary varibles u and i are used to replace the square of node voltage and branch current magnitudes. Thus, constraints (2)-(3), (6)-(7), (9), (12), (14)-(15), (17), (28)-(31) can be linearized as contraints (41)-(53).

$$\sum_{ij\in\Omega_{\mathrm{AC}}}\left(P_{\mathrm{AC},ij,t}-R_{ij}i_{\mathrm{AC},ij,t}\right)+P_{\mathrm{AC},j,t}=\sum_{jk\in\Omega_{\mathrm{AC}}}P_{\mathrm{AC},jk,t} \quad (41)$$

$$\sum_{ij\in\Omega_{\mathrm{AC}}}\left(Q_{\mathrm{AC},ij,t}-X_{ij}i_{\mathrm{AC},ij,t}\right)+Q_{\mathrm{AC},j,t}=\sum_{jk\in\Omega_{\mathrm{AC}}}Q_{\mathrm{AC},jk,t} \quad (42)$$

$$\begin{aligned}&u_{\mathrm{AC},i,t}-u_{\mathrm{AC},j,t}-2\left(R_{ij}P_{\mathrm{AC},ij,t}+X_{ij}Q_{\mathrm{AC},ij,t}\right)\\&+\left(R_{ij}^2+X_{ij}^2\right)i_{\mathrm{AC},ij,t}+\mathrm{M}\left(1-\alpha_{\mathrm{AC},ij}\right)\geq 0\end{aligned} \quad (43)$$

$$\begin{aligned}&u_{\mathrm{AC},i,t}-u_{\mathrm{AC},j,t}-2\left(R_{ij}P_{\mathrm{AC},ij,t}+X_{ij}Q_{\mathrm{AC},ij,t}\right)\\&+\left(R_{ij}^2+X_{ij}^2\right)i_{\mathrm{AC},ij,t}-\mathrm{M}\left(1-\alpha_{\mathrm{AC},ij}\right)\leq 0\end{aligned} \quad (44)$$

$$0\leq i_{\mathrm{AC},ij,t}\leq \mathrm{M}\alpha_{\mathrm{AC},ij} \quad (45)$$

$$\sum_{mn\in\Omega_{\mathrm{DC}}}\left(P_{\mathrm{DC},mn,t}-R_{mn}i_{DC,mn,t}\right)+P_{\mathrm{DC},n,t}=\sum_{nk\in\Omega_{\mathrm{DC}}}P_{\mathrm{DC},nk,t} \quad (46)$$

$$\begin{aligned}&u_{\mathrm{DC},m,t}-u_{\mathrm{DC},n,t}-2R_{mn}P_{\mathrm{DC},mn,t}\\&+R_{mn}^2i_{\mathrm{DC},mn,t}+\mathrm{M}\left(1-\alpha_{\mathrm{DC},mn}\right)\geq 0\end{aligned} \quad (47)$$

$$\begin{aligned}&u_{\mathrm{DC},m,t}-u_{\mathrm{DC},n,t}-2R_{mn}P_{\mathrm{DC},mn,t}\\&+R_{mn}^2i_{\mathrm{DC},mn,t}-\mathrm{M}\left(1-\alpha_{\mathrm{DC},mn}\right)\leq 0\end{aligned} \quad (48)$$

$$0\leq i_{\mathrm{DC},mn,t}\leq \mathrm{M}\alpha_{\mathrm{DC},mn} \quad (49)$$

$$\left(U_{\mathrm{AC}}^{\min}\right)^2\leq u_{\mathrm{AC},i,t}\leq\left(U_{\mathrm{AC}}^{\max}\right)^2 \quad (50)$$

$$\left(U_{\mathrm{DC}}^{\min}\right)^2\leq u_{\mathrm{DC},m,t}\leq\left(U_{\mathrm{DC}}^{\max}\right)^2 \quad (51)$$

$$0\leq i_{\mathrm{AC},ij,t}\leq\left(I_{\mathrm{AC}}^{\max}\right)^2 \quad (52)$$

$$0\leq i_{\mathrm{DC},mn,t}\leq\left(I_{\mathrm{DC}}^{\max}\right)^2 \quad (53)$$

The power flow constraints (8) and (16) can be converted into standard second-order cone constraints by relaxation, as follows:

$$\left\|\begin{matrix}2P_{\mathrm{AC},ij,t}\\2Q_{\mathrm{AC},ij,t}\\i_{\mathrm{AC},ij,t}-u_{\mathrm{AC},i,t}\end{matrix}\right\|_2\leq i_{\mathrm{AC},ij,t}+u_{\mathrm{AC},i,t} \quad (54)$$

$$\left\|\begin{matrix}2P_{\mathrm{DC},mn,t}\\i_{\mathrm{DC},mn,t}-u_{\mathrm{DC},m,t}\end{matrix}\right\|_2\leq i_{\mathrm{DC},mn,t}+u_{\mathrm{DC},m,t} \quad (55)$$

For the operation constraint of CDG, constraint (34) can be transformed into the rotating cone constraint, shown as:

$$\left(P_{i,t}^{\mathrm{CDG}}\right)^2+\left(Q_{i,t}^{\mathrm{CDG}}\right)^2\leq 2\frac{S_i^{\mathrm{CDG}}}{\sqrt{2}}\frac{S_i^{\mathrm{CDG}}}{\sqrt{2}} \quad (56)$$

Thus, the compact form of service restoration model is denoted as follows:

$$\begin{cases}\max f\\ s.t.\,(4)-(5),(10)-(11),(13),(18)-(21)\\(23)-(27),(32)-(33),(35)-(56)\end{cases} \quad (57)$$

3. CASE STUDY

3.1 Modified IEEE 33-node system

In this section, the fault recovery method of the HDN is analyzed and verified on a modified IEEE 33-node test feeder. The system contains 32 lines and 4 tie switches. The voltage level is 12.66kV, the total active load is 3715.0 kW, and the total reactive load is 1130.0 kvar. M is a sufficiently large constant, which is set as 1e3 in this paper. It is noted that the black solid circle denotes the AC node, and the blue solid circle denotes the DC node. The red solid and dotted lines represent the AC and DC tie switches, respectively. The test case is shown in Fig. 2. The daily PV output and loads curves are obtained from Ref. [12], as shown in Fig. 3. To consider the priority of loads in the service restoration, the weight coefficients of loads are presented in Table 1. Category I and II loads are defined as critical loads in this paper.

Two PVs are installed at nodes 13 and 33, respectively. The capacity of each PV is 300.0 kW. Three CDGs are installed at nodes 5, 9, and 27, respectively. The capacity of each CDG is 300.0 kVA, of which the minimum power factor is 0.9. Two ESSs are installed at nodes 11 and 32, respectively. The maximum value of charging and discharging power is 300.0 kW, and the upper and lower limit of energy storage of ESS are 0.36 MWh and 1.62 MWh, respectively. The charging and discharging efficiencies are 0.9381.

The proposed model is implemented in the YALMIP optimization toolbox using MATLAB R2021a and solved by the GUROBI solver. The numerical experiments are performed on a laptop with an Intel Core i5-7300 CPU processor running at 2.50 GHz and 8 GB of RAM.

TABLE 1. Weight coefficient of load

Category	Weight coefficient	Node of load
I	100	5, 11, 13, 20, 21, 27
II	10	4, 7, 9, 15, 18, 19, 23, 32, 33
III	1	1, 2, 3, 6, 8, 10, 12, 14, 16, 17, 22, 24, 25, 26, 28, 29, 30, 31

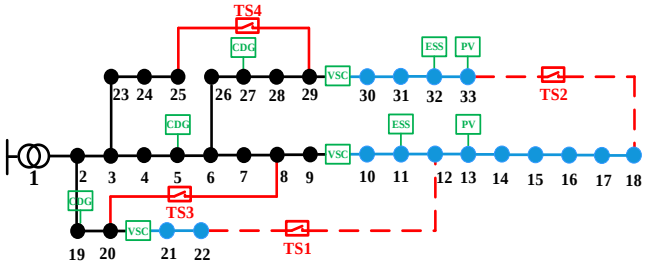

Fig. 2. Structure of the modified IEEE 33-node system

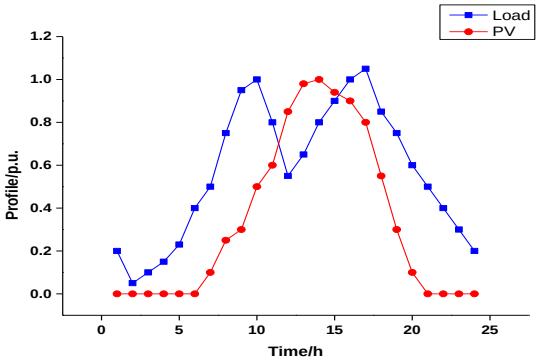

Fig. 3. Operation curves of PVs and loads

3.2 Result analysis of supply restoration

It is assumed that branch 1-2 has a permanent three-phase fault at 6:00 a.m, and the fault will last 4h. Loads of node 2 to node 33 are all out of service after the fault isolation, and the total loss of active power is 3715 kW. Two schemes are selected to conduct islanding partition and service the critical loads.

Scheme I: Supply restoration is conducted only considering DGs.

Scheme II: Supply restoration is conducted based on the coordination of DGs and ESSs.

The supply restoration results of two schemes are shown in Table 2. And the results of islanding partition in two schemes are shown in Figs. 4-5. It is noted that the gray shaded regions represent the formed islands. The solid circle indicates that the node is restored, while others are marked with a hollow one. The green solid rectangle represents the node is chosen as the voltage support point.

TABLE 2. Supply restoration results of two scheme

Scheme	Restored Load (MWh)	Recovery ratio (%)	Recovery ratio of critical load (%)	Nodes without restoration	Node with voltage support
I	2.365	63.67%	99.43%	2, 7, 24, 25, 32	5, 19
II	3.145	74.70%	100.00%	2, 24, 25	11, 19, 27

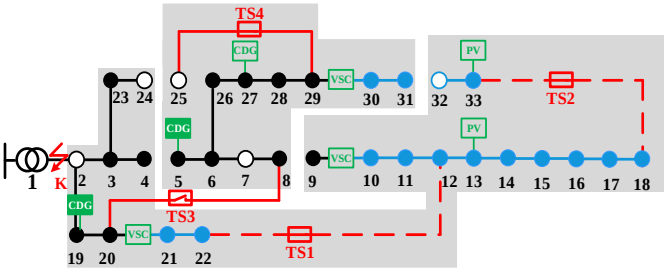

Fig. 4. Islanding partition strategy in Scheme I

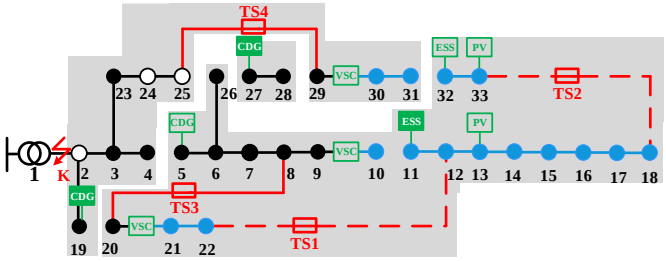

Fig. 5. Islanding partition strategy in Scheme II

In Scheme I, the load recovery rate reaches 63.97%. The original network is partitioned into two isolated islands that are energized by local CDGs, where nodes 5 and 19 are selected as voltage support points. Compared Scheme II with Scheme I, the load recovery rate increases from 63.97% to 74.70%. More loads from outages can be recovered through the coordination of ESSs and CDGs. Nodes 19 and 27 are chosen as voltage support points on the AC side, while node 11 services as the voltage support point on the DC side. The service restoration of the distribution network is effectively improved.

In addition, it also can be seen that the recovery rates of critical loads are all at a high level in both Schemes. Through setting reasonable load weight coefficients of active distribution networks, the service recovery strategy will meet different demands of various customers in actual operation, with restoring critical loads in priority.

4. CONCLUSION

This paper presents a service recovery strategy that coordinates multiple sources for HDNs with island partition. An island partition-based recovery model is proposed to guarantee critical loads' supply, by which the optimal island formulation and controllable facilities' schedule can be formed. And the model is tracked into an MISOCP to obtain an efficient and accurate solution performance. Furthermore, a modified 33-node AC/DC test feeder is used to demonstrate the effectiveness and superiority of this strategy. Results show that the proposed method realizes the sustained restoration of

critical loads and improves the reliability of the HDN in case of emergencies.

ACKNOWLEDGEMENT

This work was financially supported by the Fundamental Research Funds for the Central Universities (NO. 2021QN1066).

REFERENCE

[1] Gholami A, Aminifar F. A hierarchical response-based approach to the load restoration problem. IEEE Transactions on Smart Grid 2017; 8(4): 1700-1709.

[2] Liang Y, Niu D, Hong WC. Short term load forecasting based on feature extraction and improved general regression nerural network model. Energy 2019; 166; 653-663.

[3] Nejad RR, Sun W. Distributed load restoration in unbalanced active distribution systems. IEEE Transactions on Smart Grid 2019; 10(5): 5759-5769.

[4] Pham TTH, Besanger Y, Hadjsaid N. New challenges in power system restoration with large scale of dispersed generation insertion. IEEE Transactions on Power Systems 2009; 24(1): 398-406.

[5] Sharma A, Srinivasan D, Trivedi A. A decentralized multiagent system approach for service restoration using DG islanding. IEEE Transactions on Smart Grid 2015; 6(6): 2784-2793.

[6] Kwasinski A. Quantitative evaluation of DC microgrids availability: Effects of system architecture and converter topology design choices. IEEE Transactions on Power Electronics 2011; 26(3): 835-851.

[7] Zhang P, Li WY. Boundary analysis of distribution reliability and economic assessment. IEEE Transactions on Power Systems 2010; 25(2): 714-721.

[8] Ma TX, Wang CY, Jia JR, Duan X, et al. Fault recovery method for AC/DC hybrid distribution network based on binary particle swarm optimization algorithm. Power System Protection and Control 2019; 47(9): 112-119.

[9] Wu T, Wang JH, Lu XN, Du YH. AC/DC hybrid distribution network reconfiguration with microgrid formation using multi-agent soft actor-critic. Applied Energy 2022; 307: 118189.

[10] Yin H, Liu YB, Gao HJ, Yuan XD, et al. Load recovery strategy of AC/DC hybrid distribution network with distribution energy storage systems. Electric Power Automation Equipment 2021; 41(8): 25-32.

[11] Sun X, Qiu XY, Zhang ZR, Ren H, et al. Distribution Robust Optimal Dispatching of AC/DC Distribution Network Based on Data Driven. Power System Technology 2021; 45(12): 4768-4778.

[12] Ji HR, Wang CS, Li P, Song GY, et al. SOP-based islanding partition method of active distribution networks considering the characteristics of DG, energy storage system and load. Energy 2018; 155: 312-325.